4. MAGNETIC PROPERTIES AND THEIR IMPLICATIONS AT SITE 1007[1]

Kohsaku Arai[2] and Tokiyuki Sato[3]

ABSTRACT

A detailed rock magnetic study was conducted on the top six cores (above 57.5 meters below seafloor) at Site 1007. The calcareous nannofossil biostratigraphy assigns the studied intervals to an age ranging from early Pleistocene to Holocene. We found two significant conversion points in the Pleistocene based on isothermal remanent magnetization (IRM) acquisition and on alternating field demagnetization of anhysteretic remanent magnetization and IRM. These conversion points correlate strongly with changes in sedimentation rate and lithology. We conclude that the paleomagnetic signals reflect changes of rate of sediment supply and of paleoenvironment on the western edge of the Great Bahama Bank.

INTRODUCTION

Site 1007 is situated at 24°30.261′N, 79°19.34′W, at a water depth of 647 m on the toe-of-slope of the western Great Bahama Bank (Fig. 1). Site 1007 was positioned distal of progradational sequences and at the critical point of thinning clinoforms. Seismic refraction surveys (Eberli and Ginsburg, 1987; Eberli, Swart, Malone, et al., 1997) show sequences of thinning clinoforms both westward from the bank and eastward from the basin. The sequences at the site are composed of both drift sediment and neritic carbonate grains derived from the bank (Eberli, Swart, Malone, et al., 1997). Packages of sequences are expected at both the basinal and proximal slope sites at this position. Changes in these packages could possibly reflect the oceanic conditions of the slope of the Great Bahama Bank. Regarding oceanic conditions, the main objectives of this study were to determine the changes of sediments and their lithofacies in order to estimate accurate dates for points marking alterations in oceanic condition. Microfossils with good preservation were better observed at this site than at the proximal Sites 1005, 1004, and 1003.

Rock magnetic measurements were carried out and used as a tool for signaling the anticipated oceanic changes. They provide information about the variability of concentration, grain size, and composition of magnetic minerals within the sediment (e.g., Bloemendal et al., 1988; Thompson and Oldfield, 1986). Variations in magnetic remanence are in some cases strongly correlated with oxygen isotopic composition and $CaCO_3$ content of deep-sea cores (e.g., Kent, 1982; Bloemendal and de Menocal, 1989). The species, grain size, and concentration of magnetic minerals in the sediment on the toe-of-slope of the western Great Bahama Bank are discussed in this chapter.

MATERIAL AND METHODS

Three holes were cored at Site 1007: 1007A, 1007B, and 1007C. Onboard samples for magnetic studies were collected continuously in 7-cm^3 cubes at Hole 1007B at ~20-cm intervals in the top six cores (above 57.5 meters below seafloor [mbsf]). The sampling interval mainly consists of nannofossil ooze and variably lithified wackestone to packstone. Nannofossil ooze lithofacies dominate above 10.9 mbsf

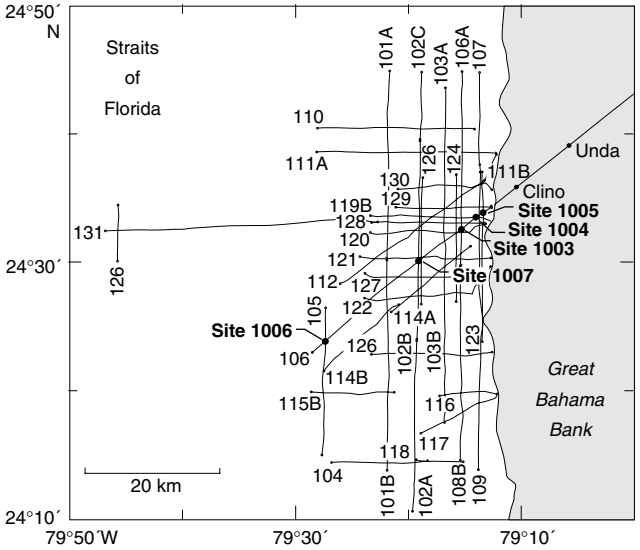

Figure 1. Location of sites drilled during Leg 166 (after Eberli, Swart, Malone, et al., 1997).

in the section. Grainstone to packstone lithofacies measuring several tens of centimeters and apparently formed by turbidity currents also appear in this interval. Each of these turbidites is marked by a sharp basal contact that is overlain by bioclastic coarse grains fining upward into wackestone. The interval from 10.9 to 43.5 mbsf consists of a sequence of nannofossil ooze that grades downhole into unlithified mudstone and wackestone. In the upper part, light olive-brown silty peloidal wackestone alternates with white nannofossil ooze. In the lower part, unlithified to partially lithified bioclastic wackestone alternates with gray-colored clay and silt-rich unlithified mudstone. Below 43.5 mbsf, unlithified peloidal wackestone lithofacies dominate.

The remanent magnetization of discrete samples was measured using a 2G Enterprises model 760 superconducting pass-through magnetometer. Stepwise alternating field (AF) demagnetization was performed to examine the stability of the remanent magnetization. Subsequently, an anhysteretic remanent magnetization (ARM) was imparted by an AF of 100 mT superimposed on a direct-current field of 0.05 mT. We examined AF demagnetization of this ARM, together with isothermal remanent magnetization (IRM) acquisition and AF demagnetization. Magnetic susceptibility was also measured with a KappaBridge KLY-3S magnetic susceptibility meter.

[1]Swart, P.K., Eberli, G.P., Malone, M.J., and Sarg, J.F. (Eds.), 2000. *Proc. ODP, Sci. Results,* 166: College Station TX (Ocean Drilling Program).
[2]Marine Geology Department, Geological Survey of Japan, 1-1-3 Higashi, Tsukuba, Ibaraki, 305-8567, Japan. kohsaku@gsj.go.jp
[3]Institute of Applied Earth Sciences, Mining College, Akita University, Tegata Gakuencho 1-1, Akita 010, Japan.

After measuring magnetic properties, each sample was processed by a smear-slide preparation method for calcareous nannofossil study. The microslide was observed under binocular polarizing.

DATING

The paleomagnetic signal derived from sediments at Site 1007 was not strong enough to provide stratigraphic control except above 2 mbsf. Well-preserved calcareous nannofossils were recovered throughout the section. We found nine calcareous nannofossil events defined by Takayama and Sato (1987). The bottom acme zone of *Emiliania huxleyi* (0.08 Ma) and the top of *Pseudoemiliania lacunosa* (0.41 Ma) are located between Samples 166-1007B-1H-2, 39 cm, and 1H-2, 59 cm. The sharp basal contact of turbidite is situated in this interval. A hiatus between 0.08 and 0.41 Ma (at least) is assumed at this sharp erosional contact. The top of *Reticulofenestra asanoi* (0.85 Ma) is located between Samples 166-1007B-1H-3, 24 cm, and 1H-3, 59 cm. The bottom of *Gephyrocapsa parallela* (0.95 Ma) is observed between Samples 166-1007B-1H-4, 24 cm, and 1H-4, 39 cm. The bottom of *R. asanoi* (1.16 Ma) occurs between Samples 166-1007B-1H-CC, and 2H-1, 19 cm. The top of large *Gephyrocapsa* (1.20 Ma) is found between Samples 166-1007B-2H-3, 39 cm, and 2H-3, 59 cm. The bottom of large *Gephyrocapsa* (1.44 Ma) is observed between Samples 166-1007B-5H-3, 13 cm, and 5H-3, 23 cm. The bottom of *Gephyrocapsa oceanica* (1.65 Ma) occurs between Samples 166-1007B-4H-1, 59 cm, and 4H-1, 99 cm. The bottom of *Gephyrocapsa caribbeanica* (1.72 Ma) is observed between Samples 166-1007B-5H-5, 133 cm, and 5H-6, 13 cm.

Figure 2 depicts the relationship between sampling depth and the datum of the calcareous nannofossil biostratigraphy. It indicates a change in sedimentation rate at least during the last 1.72 m.y. The sedimentation rate dramatically drops at depths above 12 mbsf, and there is a hiatus characterized by sharp erosional contact at 2 mbsf.

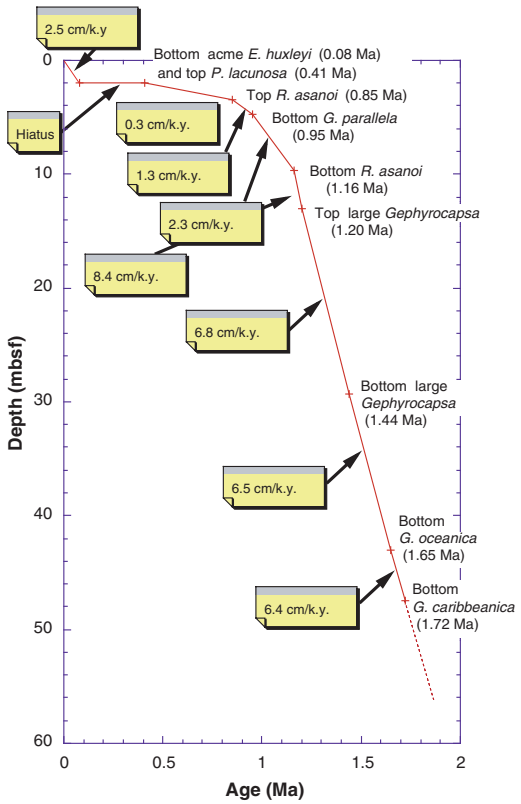

Figure 2. Age vs. depth plot for Hole 1007B based on detailed calcareous nannofossil biostratigraphy.

MAGNETIC PROPERTIES

All samples were subjected to stepwise IRM acquisition and AF demagnetization of ARM and IRM (Lowrie-Fuller test, in Lowrie and Fuller, 1971). The present sediments can be divided into four types based on the characteristics of the magnetic properties as follows (Fig. 3):

- Type 1 is characterized by a steep initial increase in the IRM acquisition curves and a lower coercivity of IRM than ARM.
- Type 2 shows a gradual rise in the IRM acquisition curves and a higher coercivity of IRM than ARM.
- Type 3 displays a relatively steep initial increase in the IRM acquisition curves and a higher coercivity of IRM than ARM.
- Type 4 is defined by a steep initial increase in the IRM acquisition curves and similar AF demagnetization curves for IRM and ARM.

The stratigraphic distribution of these types and the remanent intensity of magnetization (natural remanent magnetization [NRM], ARM, and IRM) are shown in Figure 4. Type 1 occurs above 2 mbsf and is characterized by high remanent intensity and stable normal polarity of magnetization. Type 2 is observed between 2 and 12 mbsf. Low remanent intensity of magnetization prevails in this interval. Types 3 and 4 are encountered repeatedly below 12 mbsf, and the intensity of remanent magnetization changes with them. The intensities of remanent magnetization within Type 4 tend to be higher than within Type 3.

IRM is saturated before the magnetic field reaches 0.4 T, except in Type 2 sediment. Magnetic remanent intensities of the samples placed in a magnetic field that reached 2 T were considered the saturation isothermal remanent magnetization (SIRM). IRM was also examined after application of a reversed field of 0.3 T after measuring SIRM. The S-ratio (Thompson and Oldfield, 1986) and the ratio of ARM to SIRM were calculated and are shown in Figure 4. The S-ratio reflects variation in the coercivity spectrum of the magnetic minerals (Thompson and Oldfield, 1986), and the ratio of ARM to SIRM primarily mirrors the presence of finer grained magnetic grains (King et al., 1982). Samples within Type 2 sediments showed a low S-ratio (although not saturated enough). A high S-ratio is observed within Type 4 sediments.

MAGNETIC VARIABILITY

Downcore variability of the magnetic remanent intensities is shown on the left panel in Figure 4. Except for the uppermost samples, magnetic susceptibility was diamagnetic (Table 1), which is characteristic of carbonate-dominated sediment (Eberli, Swart, Malone, et al., 1997). The variability curves of the remanent intensity of ARM and IRM are similar to each other.

We provide the variability curve of the magnetic remanent intensities on the top three cores (26.0 mbsf) at Site 1003 on the left panel in Figure 5. Site 1003 is located on the middle slope of the Great Bahama Bank and is positioned ~6 km landward of Site 1007. The bottom acme zone of *E. huxleyi* (0.08 Ma) lies between Samples 166-1003A-1H-5, 79 cm, and 2H-1, 120 cm. The bottom of *E. huxleyi* (0.25 Ma) occurs between Samples 166-1003A-2H-4, 10 cm, and 2H-4, 59 cm (Fig. 5). The top of *P. lacunosa* (0.41 Ma) is located at Core 166-1003A-7H (between 56.94 and 57.69 mbsf). A conspicuous hiatus such as in Site 1007 cannot be observed on the top three cores. Therefore, the variability curve of Site 1003 is considered as a

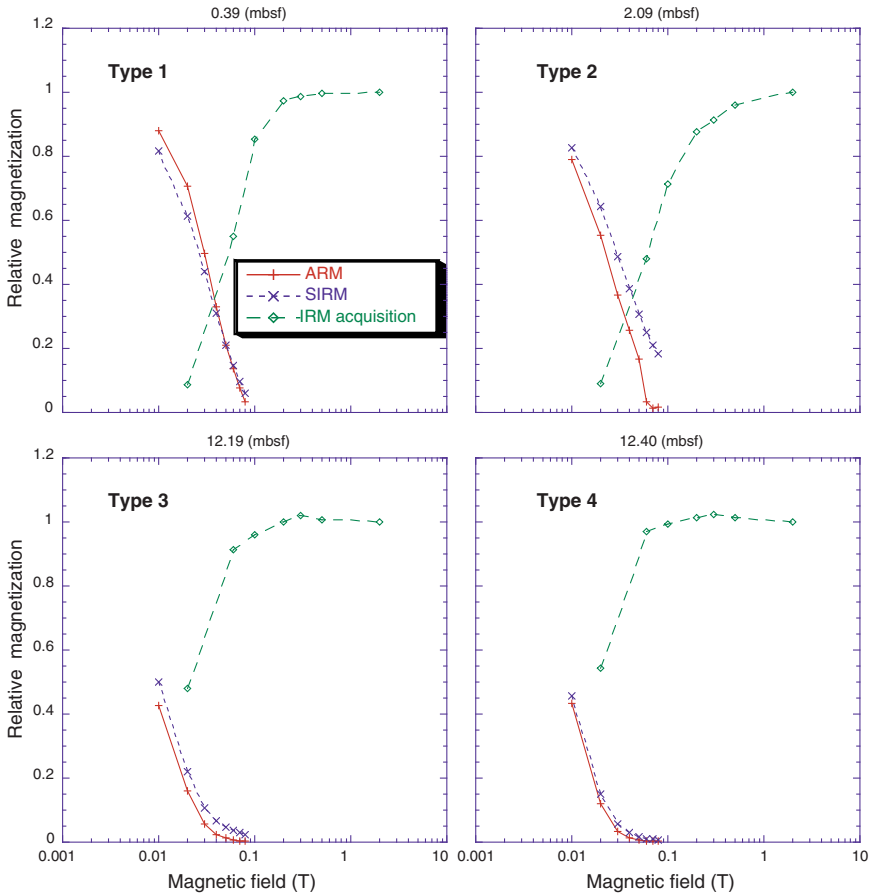

Figure 3. Coercivity spectra of the ARM and IRM and stepwise IRM acquisition. Four types are identified in this study: Type 1, a steep initial increase in the IRM acquisition curves and a lower coercivity of IRM than of ARM; Type 2, a gradual rise in the IRM acquisition curves and a higher coercivity of IRM than of ARM; Type 3, a relatively steep initial increase in the IRM acquisition curves and a higher coercivity of IRM than of ARM; and Type 4, a steep initial increase in the IRM acquisition curves and similar AF demagnetization curves for IRM and ARM. ARM = anhysteretic remanent magnetization, IRM = isothermal remanent magnetization, SIRM = saturation isothermal remanent magnetization.

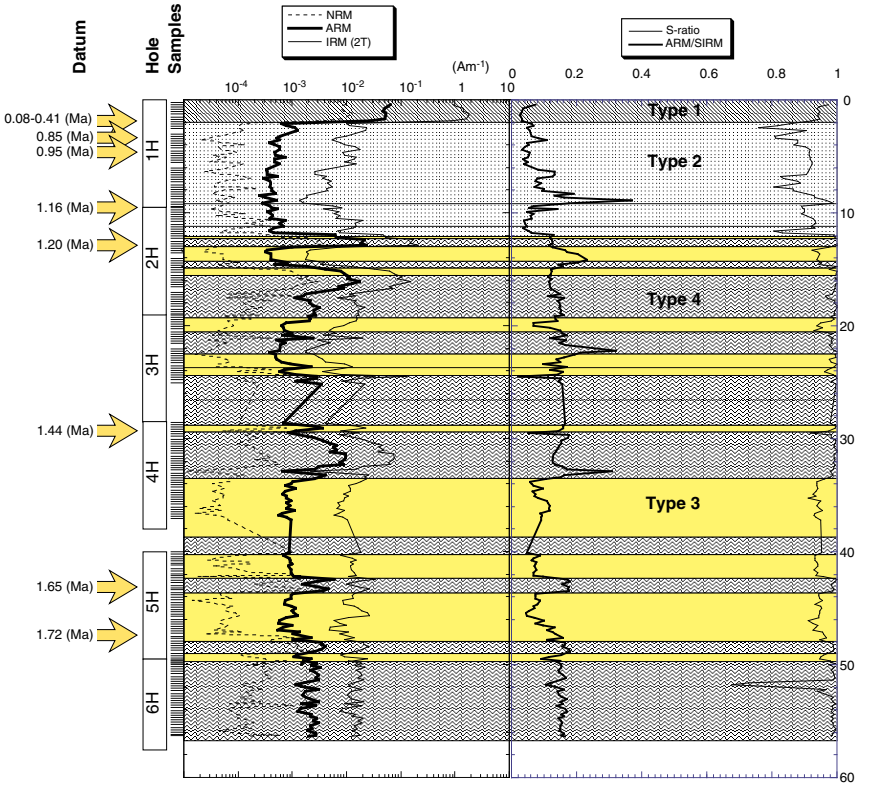

Figure 4. The stratigraphic distribution of the four types of magnetic properties (see Fig. 3) and remanent intensities. The right panel shows the S-ratio and ARM/SIRM. ARM = anhysteretic remanent magnetization, IRM = isothermal remanent magnetization, SIRM = saturation isothermal remanent magnetization, NRM = natural remanent magnetization.

Table 1. Magnetic data from Hole 1007B including the remanent intensities of NRM, ARM, IRM, the S-ratio, and ARM/SIRM.

Core, section, interval (cm)	Depth (mbsf)	NRM (A/m)	ARM (A/m)	IRM (2 T) (A/m)	Susceptibility (SI)	S-ratio	ARM/SIRM
166-1007B-							
1H-1, 19	0.19						
1H-1, 39	0.39	9.66E–03	6.62E–02	8.94E–01	3.57E–05	9.73E–01	7.40E–02
1H-1, 59	0.59	7.73E–03	5.79E–02	1.07E+00	6.32E–05	9.47E–01	5.40E–02
1H-1, 79	0.79	7.74E–03	5.01E–02	1.42E+00	1.10E–04	9.38E–01	3.53E–02
1H-1, 99	0.99	8.72E–03	4.72E–02	1.42E+00	1.01E–04	9.47E–01	3.33E–02
1H-1, 119	1.19	1.32E–02	5.41E–02	1.74E+00	1.31E–04	9.45E–01	3.11E–02
1H-1, 140	1.40	1.13E–02	5.22E–02	1.83E+00	1.43E–04	9.42E–01	2.85E–02
1H-2, 19	1.69	8.93E–03	5.14E–02	1.62E+00	1.12E–04	9.47E–01	3.17E–02
1H-2, 39	1.89	4.10E–03	2.82E–02	8.61E–01	5.65E–05	9.20E–01	3.27E–02
1H-2, 59	2.09	1.19E–04	6.24E–04	9.85E–03	–9.82E–06	8.53E–01	6.33E–02
1H-2, 79	2.29	1.02E–04	7.89E–04	1.15E–02	–9.04E–06	8.19E–01	6.84E–02
1H-2, 99	2.49	9.79E–05	1.13E–03	2.40E–02	–5.32E–06	7.58E–01	4.70E–02
1H-2, 119	2.69	1.35E–04	1.26E–03	2.23E–02	–5.98E–06	9.06E–01	5.65E–02
1H-3, 19	3.19	4.12E–05	6.18E–04	1.01E–02	–1.02E–05	8.10E–01	6.10E–02
1H-3, 39	3.39	2.69E–05	5.25E–04	6.32E–03	–1.16E–05	8.12E–01	8.31E–02
1H-3, 59	3.59	1.97E–05	5.95E–04	5.51E–03	–1.05E–05	8.81E–01	1.08E–01
1H-3, 79	3.79	5.59E–05	3.76E–04	7.78E–03	–1.05E–05	8.81E–01	4.83E–02
1H-3, 99	3.99	1.33E–04	4.78E–04	9.15E–03	–8.24E–06	8.67E–01	5.23E–02
1H-3, 119	4.19	4.39E–05	5.77E–04	1.43E–02	–6.17E–06	9.03E–01	4.02E–02
1H-3, 140	4.40	4.88E–05	5.87E–04	1.76E–02	–4.68E–06	9.19E–01	3.33E–02
1H-4, 19	4.69	9.31E–05	4.79E–04	8.48E–03	–9.17E–06	9.16E–01	5.65E–02
1H-4, 39	4.89	3.39E–05	4.91E–04	9.14E–03	–8.46E–06	9.16E–01	5.37E–02
1H-4, 59	5.09	5.92E–05	7.31E–04	1.48E–02	–6.80E–06	9.19E–01	4.93E–02
1H-4, 79	5.29	5.18E–05	4.82E–04	1.38E–02	–6.09E–06	9.17E–01	3.50E–02
1H-4, 99	5.49	3.03E–05	4.70E–04	9.38E–03	–8.77E–06	9.23E–01	5.01E–02
1H-4, 119	5.69	1.32E–04	5.90E–04	1.51E–02	–7.29E–06	9.23E–01	3.90E–02
1H-5, 19	6.19	4.30E–05	3.36E–04	3.98E–03	–1.18E–05	9.14E–01	8.44E–02
1H-5, 39	6.39	2.42E–05	3.45E–04	2.58E–03	–1.22E–05	9.13E–01	1.34E–01
1H-5, 59	6.59	5.59E–05	3.45E–04	2.62E–03	–1.22E–05	9.07E–01	1.32E–01
1H-5, 79	6.79	1.18E–04	5.37E–04	4.23E–03	–1.27E–05	8.28E–01	1.27E–01
1H-5, 99	6.99	1.71E–04	2.94E–04	3.62E–03	–1.27E–05	8.35E–01	8.11E–02
1H-5, 119	7.19	5.09E–05	3.86E–04	5.21E–03	–1.20E–05	8.80E–01	7.40E–02
1H-5, 140	7.40	3.76E–05	4.04E–04	4.37E–03	–1.22E–05	8.87E–01	9.23E–02
1H-6, 19	7.69	3.61E–05	3.94E–04	5.54E–03	–1.17E–05	8.05E–01	7.11E–02
1H-6, 39	7.89	2.29E–04	4.23E–04	4.24E–03	–1.25E–05	8.64E–01	9.97E–02
1H-6, 59	8.09	4.47E–05	4.21E–04	4.47E–03	–1.20E–05	8.68E–01	9.43E–02
1H-6, 79	8.29	3.21E–05	5.00E–04	2.64E–03	–1.26E–05	9.07E–01	1.90E–01
1H-6, 99	8.49	5.79E–05	2.44E–04	1.82E–03	–1.36E–05	9.29E–01	1.34E–01
1H-6, 119	8.69	8.88E–05	3.13E–04	1.92E–03	–1.27E–05	9.34E–01	1.63E–01
1H-6, 140	8.90	3.76E–05	5.10E–04	1.37E–03	–1.36E–05	9.69E–01	3.71E–01
1H-7, 19	9.19	6.83E–05	2.86E–04	1.61E–03	–1.35E–05	9.87E–01	1.78E–01
1H-7, 39	9.39	4.94E–05	3.94E–04	5.72E–03	–1.04E–05	8.92E–01	6.90E–02
1H-7, 59	9.59	4.03E–05	4.29E–04	8.04E–03	–9.58E–06	8.95E–01	5.34E–02
2H-1, 19	9.69	3.05E–05	5.40E–04	3.79E–03	–1.15E–05	9.00E–01	1.42E–01
2H-1, 39	9.89	5.57E–05	3.41E–04	7.15E–03	–8.88E–06	9.00E–01	4.77E–02
2H-1, 59	10.09	1.40E–04	4.04E–04	6.01E–03	–1.04E–05	8.92E–01	6.73E–02
2H-1, 79	10.29	3.76E–05	4.45E–04	7.41E–03	–9.82E–06	9.06E–01	6.00E–02
2H-1, 99	10.49	1.27E–04	3.94E–04	6.30E–03	–9.33E–06	9.27E–01	6.27E–02
2H-1, 119	10.69	4.16E–04	7.47E–04	2.01E–02	–2.37E–06	9.34E–01	3.72E–02
2H-1, 140	10.90	1.41E–04	5.81E–04	1.44E–02	–5.72E–06	9.36E–01	4.03E–02
2H-2, 19	11.19	3.83E–04	6.84E–04	1.49E–02	–5.43E–06	9.21E–01	4.59E–02
2H-2, 39	11.39	1.04E–04	4.66E–04	1.35E–02	–6.41E–06	9.33E–01	3.46E–02
2H-2, 59	11.59	4.87E–05	3.80E–04	7.01E–03	–1.20E–05	8.07E–01	5.43E–02
2H-2, 79	11.79	4.73E–05	4.62E–04	7.54E–03	–1.16E–05	8.34E–01	6.13E–02
2H-2, 99	11.99	3.99E–04	6.13E–03	4.74E–02	–4.13E–06	9.91E–01	1.29E–01
2H-2, 119	12.19	7.12E–04	6.42E–03	5.39E–02	–4.63E–06	9.95E–01	1.19E–01
2H-2, 140	12.40	3.20E–03	2.13E–02	1.72E–01	8.80E–06	1.00E+00	1.24E–01
2H-3, 19	12.69	2.62E–03	1.88E–02	1.47E–01	2.69E–06	1.00E+00	1.28E–01
2H-3, 39	12.89	3.95E–03	2.40E–02	2.07E–01	7.92E–06	9.99E–01	1.16E–01
2H-3, 59	13.09	3.52E–05	9.78E–04	7.66E–03	–1.11E–05	9.74E–01	1.28E–01
2H-3, 79	13.29	2.46E–05	3.51E–04	2.11E–03	–1.32E–05	9.24E–01	1.66E–01
2H-3, 99	13.49	2.24E–05	3.14E–04	1.85E–03	–1.32E–05	9.40E–01	1.70E–01
2H-3, 119	13.69	5.60E–05	3.99E–04	1.98E–03	–1.33E–05	9.47E–01	2.02E–01
2H-4, 19	14.19	5.32E–05	4.08E–04	1.76E–03	–1.24E–05	9.39E–01	2.32E–01
2H-4, 39	14.39	1.12E–04	7.97E–04	3.91E–03	–1.28E–05	9.54E–01	2.04E–01
2H-4, 59	14.59	4.20E–05	4.82E–04	3.35E–03	–1.33E–05	9.45E–01	1.44E–01
2H-4, 79	14.79	5.81E–05	1.81E–03	1.15E–02	–1.14E–05	1.00E+00	1.58E–01
2H-4, 99	14.99	2.25E–04	4.04E–03	3.32E–02	–5.18E–06	9.78E–01	1.21E–01
2H-4, 119	15.19	9.51E–04	7.76E–03	6.31E–02	–1.46E–06	1.00E+00	1.23E–01
2H-4, 140	15.40	1.16E–03	9.33E–03	7.67E–02	6.50E–07	9.97E–01	1.22E–01
2H-5, 19	15.69	1.92E–03	1.15E–02	1.04E–01	3.46E–06	1.00E+00	1.11E–01
2H-5, 39	15.89	1.23E–03	1.05E–02	8.58E–02	–1.24E–06	9.95E–01	1.23E–01
2H-5, 59	16.09	2.98E–03	1.74E–02	1.50E–01	5.74E–06	1.01E+00	1.16E–01
2H-5, 79	16.29	1.84E–03	1.27E–02	1.07E–01	–6.84E–07	9.98E–01	1.19E–01
2H-5, 99	16.49	1.09E–03	7.27E–03	6.20E–02	–4.80E–06	9.94E–01	1.17E–01
2H-5, 119	16.69	1.12E–03	8.72E–03	7.16E–02	–4.13E–06	9.94E–01	1.22E–01
2H-6, 19	17.19	6.65E–05	1.72E–03	1.14E–02	–1.27E–05	9.85E–01	1.51E–01
2H-6, 39	17.39	1.02E–03	1.61E–03	1.42E–02	–9.97E–06	9.64E–01	1.13E–01
2H-6, 59	17.59	5.90E–05	1.12E–03	6.88E–03	–1.24E–05	9.72E–01	1.63E–01
2H-6, 79	17.79	3.99E–04	2.12E–03	1.51E–02	–1.21E–05	9.93E–01	1.41E–01
2H-6, 99	17.99	1.25E–04	2.05E–03	1.38E–02	–1.15E–05	9.92E–01	1.48E–01
2H-6, 119	18.19	1.47E–04	2.38E–03	1.58E–02	–1.10E–05	1.00E+00	1.51E–01
2H-6, 140	18.40	2.70E–04	3.23E–03	2.18E–02	–1.07E–05	9.99E–01	1.48E–01
2H-7, 19	18.69	1.21E–04	2.51E–03	1.65E–02	–1.12E–05	9.93E–01	1.53E–01
2H-7, 39	18.89	1.38E–04	2.48E–03	1.65E–02	–1.08E–05	9.92E–01	1.51E–01
2H-7, 59	19.09	2.41E–04	2.73E–03	1.69E–02	–1.09E–05	9.93E–01	1.61E–01
3H-1, 19	19.19	5.30E–05	2.00E–03	1.49E–02	–1.00E–05	9.82E–01	1.34E–01
3H-1, 39	19.39	1.73E–04	2.10E–03	1.55E–02	–1.03E–05	9.90E–01	1.35E–01

Table 1 (continued).

Core, section, interval (cm)	Depth (mbsf)	NRM (A/m)	ARM (A/m)	IRM (2 T) (A/m)	Susceptibility (SI)	S-ratio	ARM/SIRM
3H-1, 59	19.59	6.42E–05	2.08E–03	1.49E–02	–9.70E–06	9.83E–01	1.40E–01
3H-1, 79	19.79	7.66E–05	7.83E–04	1.14E–02	–6.71E–06	9.49E–01	6.85E–02
3H-1, 99	19.99	8.15E–05	6.22E–04	8.95E–03	–8.12E–06	9.38E–01	6.95E–02
3H-1, 119	20.19	6.19E–05	6.99E–04	5.87E–03	–1.14E–05	9.57E–01	1.19E–01
3H-1, 140	20.40	4.40E–05	7.28E–04	4.89E–03	–1.08E–05	9.31E–01	1.49E–01
3H-2, 19	20.69	6.34E–05	9.99E–04	6.45E–03	–1.32E–05	9.89E–01	1.55E–01
3H-2, 39	20.89	3.34E–05	6.53E–04	3.81E–03	–1.23E–05	9.73E–01	1.72E–01
3H-2, 59	21.09	4.27E–04	2.39E–03	2.01E–02	–1.07E–05	9.89E–01	1.19E–01
3H-2, 79	21.29	2.85E–05	5.10E–04	3.02E–03	–1.39E–05	9.83E–01	1.69E–01
3H-2, 99	21.49	6.72E–05	7.45E–04	5.12E–03	–1.27E–05	9.86E–01	1.46E–01
3H-2, 119	21.69	4.42E–05	6.03E–04	3.68E–03	–1.30E–05	9.78E–01	1.64E–01
3H-3, 19	22.19	3.00E–05	5.84E–04	1.82E–03	–1.32E–05	9.92E–01	3.21E–01
3H-3, 39	22.39	2.06E–05	3.76E–04	1.78E–03	–1.33E–05	1.00E+00	2.11E–01
3H-3, 59	22.59	1.63E–05	4.94E–04	2.55E–03	–1.32E–05	9.94E–01	1.94E–01
3H-3, 79	22.79	5.16E–05	4.98E–04	3.08E–03	–1.35E–05	9.98E–01	1.61E–01
3H-3, 99	22.99	6.01E–05	5.14E–04	3.68E–03	–1.30E–05	9.78E–01	1.39E–01
3H-3, 119	23.19	7.44E–05	6.32E–04	4.18E–03	–1.22E–05	9.82E–01	1.51E–01
3H-3, 140	23.40	4.11E–05	9.05E–04	9.20E–03	–1.26E–05	9.99E–01	9.85E–02
3H-4, 19	23.69	3.90E–05	2.23E–03	1.30E–02	–1.22E–05	9.91E–01	1.71E–01
3H-4, 39	23.89	4.01E–04	7.05E–04	6.05E–03	–1.31E–05	9.72E–01	1.17E–01
3H-4, 59	24.09	9.03E–05	5.72E–04	3.61E–03	–1.26E–05	9.61E–01	1.59E–01
3H-4, 79	24.29	5.46E–04	1.11E–03	7.92E–03	–1.16E–05	9.87E–01	1.40E–01
3H-4, 99	24.49	3.39E–02	2.81E–03	1.29E–01	9.14E–06	9.98E–01	2.18E–02
3H-4, 119	24.69	8.20E–05	2.81E–03	1.84E–02	–1.05E–05	9.99E–01	1.52E–01
3H-4, 140	24.90	1.39E–04	1.18E–03	8.16E–03	–1.19E–05	9.84E–01	1.45E–01
3H-5, 19	25.19	2.48E–04	3.42E–03	2.20E–02	–9.88E–06	9.96E–01	1.56E–01
4H-1, 19	28.69	1.04E–04	6.78E–04	4.10E–03	–1.35E–05	9.79E–01	1.65E–01
4H-1, 39	28.89	2.62E–04	2.47E–03	1.56E–02	–1.12E–05	9.98E–01	1.58E–01
4H-1, 59	29.09	7.86E–04	3.66E–03	2.29E–02	–1.09E–05	9.94E–01	1.60E–01
4H-1, 79	29.29	5.26E–05	1.15E–03	7.90E–03	–1.11E–05	9.73E–01	1.45E–01
4H-1, 99	29.49	2.75E–03	8.58E–04	1.70E–02	–1.07E–05	9.17E–01	5.06E–02
4H-1, 119	29.69	1.31E–04	1.32E–03	7.44E–03	–1.30E–05	9.83E–01	1.78E–01
4H-1, 140	29.90	2.45E–04	2.54E–03	1.45E–02	–1.18E–05	9.82E–01	1.75E–01
4H-2, 19	30.19	1.53E–04	3.63E–03	2.37E–02	–1.07E–05	9.96E–01	1.53E–01
4H-2, 40	30.40	9.19E–05	5.01E–03	3.25E–02	–9.83E–06	9.94E–01	1.54E–01
4H-2, 59	30.59	1.49E–04	6.60E–03	4.50E–02	–9.00E–06	9.91E–01	1.47E–01
4H-2, 80	30.80	1.91E–04	5.74E–03	4.00E–02	–9.82E–06	9.92E–01	1.43E–01
4H-2, 99	30.99	2.13E–04	6.78E–03	4.95E–02	–9.09E–06	9.99E–01	1.37E–01
4H-2, 119	31.19	2.31E–04	5.08E–03	3.76E–02	–9.65E–06	1.00E+00	1.35E–01
4H-2, 140	31.40	2.89E–04	9.77E–03	7.47E–02	–6.56E–06	9.92E–01	1.31E–01
4H-3, 19	31.69	3.83E–04	9.55E–03	7.50E–02	–5.88E–06	9.92E–01	1.27E–01
4H-3, 39	31.89	1.91E–04	9.15E–03	7.23E–02	–6.30E–06	9.94E–01	1.27E–01
4H-3, 59	32.09	5.62E–04	7.63E–03	5.98E–02	–6.69E–06	9.88E–01	1.27E–01
4H-3, 79	32.29	5.36E–04	8.86E–03	6.52E–02	–7.07E–06	9.93E–01	1.36E–01
4H-3, 99	32.49	1.83E–04	3.15E–03	2.01E–02	–1.16E–05	9.91E–01	1.56E–01
4H-3, 119	32.69	7.21E–05	2.61E–03	1.52E–02	–1.23E–05	9.89E–01	1.72E–01
4H-3, 138	32.88	1.12E–05	6.64E–04	2.16E–03	–1.34E–05	9.80E–01	3.08E–01
4H-4, 19	33.19	1.31E–04	4.10E–03	2.52E–02	–9.61E–06	9.87E–01	1.63E–01
4H-4, 39	33.39	7.95E–05	3.29E–03	2.15E–02	–9.66E–06	9.81E–01	1.53E–01
4H-4, 59	33.59	6.76E–05	2.51E–03	2.37E–02	–4.24E–06	9.61E–01	1.06E–01
4H-4, 80	33.80	7.57E–05	1.03E–03	1.88E–02	–1.69E–06	9.38E–01	5.50E–02
4H-4, 99	33.99	3.36E–05	9.37E–04	1.49E–02	–3.80E–06	9.39E–01	6.29E–02
4H-4, 119	34.19	4.22E–05	7.59E–04	1.11E–02	–5.69E–06	9.37E–01	6.82E–02
4H-4, 140	34.40	5.80E–05	1.15E–03	1.20E–02	–6.14E–06	9.41E–01	9.56E–02
4H-5, 19	34.69	3.13E–05	7.46E–04	1.16E–02	–5.99E–06	9.36E–01	6.46E–02
4H-5, 39	34.89	5.93E–05	6.70E–04	8.93E–03	–5.76E–06	9.28E–01	7.50E–02
4H-5, 59	35.09	5.27E–05	7.75E–04	1.07E–02	–6.21E–06	9.35E–01	7.24E–02
4H-5, 79	35.29	5.39E–05	7.68E–04	9.34E–03	–7.80E–06	9.11E–01	8.23E–02
4H-5, 99	35.49	3.20E–05	9.58E–04	8.77E–03	–8.15E–06	9.49E–01	1.09E–01
4H-5, 119	35.69	4.37E–05	7.80E–04	7.05E–03	–9.64E–06	9.43E–01	1.11E–01
4H-5, 140	35.90	4.75E–05	9.11E–04	7.68E–03	–8.28E–06	9.39E–01	1.19E–01
4H-6, 19	36.19	1.89E–05	7.80E–04	6.77E–03	–1.01E–05	9.47E–01	1.15E–01
4H-6, 39	36.39	5.06E–05	1.10E–03	9.34E–03	–8.28E–06	9.57E–01	1.17E–01
4H-6, 59	36.59	1.55E–05	6.48E–04	7.31E–03	–8.60E–06	9.34E–01	8.86E–02
4H-6, 79	36.79	3.80E–05	5.66E–04	6.01E–03	–6.81E–06	9.30E–01	9.41E–02
4H-6, 99	36.99	6.36E–05	7.73E–04	8.45E–03	–2.95E–06	9.35E–01	9.15E–02
4H-6, 119	37.19	6.50E–05	9.53E–04	1.05E–02	–4.19E–06	9.49E–01	9.07E–02
5H-1, 13	40.13	1.07E–03	8.89E–04	1.87E–02	–5.16E–06	9.52E–01	4.77E–02
5H-1, 33	40.33	1.25E–04	6.97E–04	7.86E–03	–7.96E–06	9.34E–01	8.87E–02
5H-1, 57	40.57	3.84E–05	8.65E–04	1.30E–02	–4.96E–06	9.34E–01	6.66E–02
5H-1, 75	40.75	2.79E–05	9.29E–04	1.49E–02	–3.35E–06	9.33E–01	6.22E–02
5H-1, 93	40.93	1.72E–04	9.03E–04	1.17E–02	–4.93E–06	9.38E–01	7.72E–02
5H-1, 115	41.15	1.69E–04	9.86E–04	1.33E–02	–3.99E–06	9.41E–01	7.41E–02
5H-1, 130	41.30	3.34E–05	8.30E–04	1.19E–02	–4.48E–06	9.40E–01	6.97E–02
5H-2, 13	41.63	1.10E–04	9.66E–04	1.24E–02	–4.80E–06	9.30E–01	7.79E–02
5H-2, 33	41.83	1.72E–04	9.53E–04	1.37E–02	–4.19E–06	9.42E–01	6.94E–02
5H-2, 59	42.09	1.46E–03	1.01E–03	1.51E–02	–4.95E–06	9.36E–01	6.68E–02
5H-2, 74	42.24	1.81E–05	1.06E–03	1.11E–02	–5.38E–06	9.60E–01	9.57E–02
5H-2, 93	42.43	1.42E–03	5.82E–03	3.43E–02	–9.52E–06	9.99E–01	1.70E–01
5H-2, 115	42.65	7.40E–04	2.95E–03	1.63E–02	–1.10E–05	9.95E–01	1.81E–01
5H-2, 135	42.85	2.06E–04	1.56E–03	1.01E–02	–1.19E–05	9.84E–01	1.55E–01
5H-3, 13	43.13	4.15E–04	2.96E–03	1.67E–02	–1.16E–05	9.86E–01	1.77E–01
5H-3, 33	43.33	1.50E–03	4.58E–03	2.62E–02	–1.06E–05	9.91E–01	1.75E–01
5H-3, 48	43.48	1.37E–03	3.70E–03	2.07E–02	–1.08E–05	9.86E–01	1.78E–01
5H-3, 75	43.75	4.68E–05	1.03E–03	1.38E–02	–4.78E–06	9.45E–01	7.49E–02
5H-3, 93	43.93	4.81E–05	9.43E–04	1.29E–02	–4.69E–06	9.45E–01	7.31E–02
5H-3, 115	44.15	7.87E–05	9.50E–04	1.31E–02	–3.68E–06	9.46E–01	7.28E–02
5H-3, 137	44.37	1.45E–05	7.57E–04	8.55E–03	–6.17E–06	9.56E–01	8.85E–02
5H-4, 13	44.63	4.48E–05	7.16E–04	8.91E–03	–5.75E–06	9.34E–01	8.03E–02

Table 1 (continued).

Core, section, interval (cm)	Depth (mbsf)	NRM (A/m)	ARM (A/m)	IRM (2 T) (A/m)	Susceptibility (SI)	S-ratio	ARM/SIRM
5H-4, 33	44.83	8.14E–05	9.48E–04	1.40E–02	–3.75E–06	9.49E–01	6.79E–02
5H-4, 53	45.03	6.26E–05	1.15E–03	1.63E–02	–2.14E–06	9.52E–01	7.04E–02
5H-4, 75	45.25	5.54E–05	9.85E–04	1.90E–02	6.51E–07	9.47E–01	5.17E–02
5H-4, 93	45.43	9.05E–05	1.06E–03	2.41E–02	5.41E–06	9.47E–01	4.38E–02
5H-4, 115	45.65	1.10E–04	1.24E–03	2.67E–02	7.01E–06	9.45E–01	4.64E–02
5H-4, 133	45.83	8.12E–05	7.76E–04	1.08E–02	–5.23E–06	9.45E–01	7.17E–02
5H-5, 13	46.13	4.64E–05	5.90E–04	5.94E–03	–1.14E–05	9.11E–01	9.94E–02
5H-5, 33	46.33	4.60E–05	5.56E–04	7.50E–03	–8.66E–06	9.27E–01	7.42E–02
5H-5, 52	46.52	6.63E–05	9.85E–04	1.00E–02	–7.31E–06	9.41E–01	9.85E–02
5H-5, 73	46.73	5.72E–05	6.73E–04	5.10E–03	–9.09E–06	9.35E–01	1.32E–01
5H-5, 93	46.93	3.59E–05	5.32E–04	4.85E–03	–9.08E–06	9.26E–01	1.10E–01
5H-5, 113	47.13	1.24E–04	1.39E–03	1.09E–02	–7.84E–06	9.57E–01	1.28E–01
5H-5, 133	47.33	2.47E–05	1.04E–03	7.68E–03	–8.44E–06	9.59E–01	1.35E–01
5H-6, 13	47.63	1.06E–03	2.21E–03	1.39E–02	–8.45E–06	9.67E–01	1.59E–01
5H-6, 28	47.78	4.26E–04	1.03E–03	9.36E–03	–7.31E–06	9.47E–01	1.10E–01
5H-6, 53	48.03	3.75E–04	3.46E–03	2.08E–02	–1.03E–05	9.79E–01	1.66E–01
5H-6, 73	48.23	1.42E–03	3.48E–03	2.11E–02	–1.16E–05	9.89E–01	1.65E–01
5H-6, 93	48.43	1.24E–03	4.06E–03	2.58E–02	–1.09E–05	9.88E–01	1.57E–01
5H-6, 113	48.63	1.17E–03	3.46E–03	1.97E–02	–1.01E–05	9.90E–01	1.76E–01
5H-6, 133	48.83	2.03E–03	2.76E–03	1.54E–02	–1.11E–05	9.87E–01	1.79E–01
5H-7, 13	49.13	1.13E–04	1.20E–03	7.85E–03	–9.04E–06	9.60E–01	1.52E–01
5H-7, 33	49.33	1.36E–04	1.08E–03	9.33E–03	–9.04E–06	9.51E–01	1.15E–01
5H-7, 53	49.53	3.20E–04	2.23E–03	2.43E–02	–1.23E–06	9.47E–01	9.19E–02
5H-CC, 13	49.77	3.57E–04	1.62E–03	1.09E–02	–1.16E–05	9.80E–01	1.49E–01
5H-CC, 33	49.97	1.88E–04	1.49E–03	1.08E–02	–1.09E–05	9.75E–01	1.37E–01
6H-1, 19	49.69	7.73E–04	1.62E–03	1.09E–02	–1.26E–05	9.80E–01	1.49E–01
6H-1, 39	49.89	2.39E–04	2.87E–03	1.90E–02	–1.19E–05	9.94E–01	1.52E–01
6H-1, 59	50.09	1.45E–04	2.19E–03	1.42E–02	–1.20E–05	9.83E–01	1.54E–01
6H-1, 79	50.29	3.63E–04	3.35E–03	2.19E–02	–1.15E–05	9.92E–01	1.53E–01
6H-1, 99	50.49	4.29E–04	2.15E–03	1.48E–02	–1.17E–05	9.82E–01	1.45E–01
6H-1, 119	50.69	2.83E–04	2.62E–03	1.79E–02	–1.18E–05	9.88E–01	1.47E–01
6H-1, 140	50.90	3.36E–04	3.10E–03	1.96E–02	–1.17E–05	9.92E–01	1.58E–01
6H-2, 19	51.19	4.20E–04	2.76E–03	1.63E–02	–1.17E–05	9.95E–01	1.69E–01
6H-2, 39	51.39	3.11E–04	3.11E–03	2.06E–02	–1.19E–05	9.88E–01	1.51E–01
6H-2, 59	51.59	2.02E–04	1.68E–03	1.37E–02	–1.31E–05	7.30E–01	1.22E–01
6H-2, 79	51.79	1.13E–04	1.15E–03	1.10E–02	–1.27E–05	6.78E–01	1.05E–01
6H-2, 99	51.99	1.67E–04	1.49E–03	1.13E–02	–1.22E–05	8.02E–01	1.33E–01
6H-2, 119	52.19	2.92E–04	3.13E–03	1.95E–02	–1.14E–05	9.68E–01	1.61E–01
6H-2, 140	52.40	1.40E–04	1.78E–03	1.25E–02	–1.32E–05	9.41E–01	1.42E–01
6H-3, 19	52.69	1.86E–04	1.55E–03	1.06E–02	–1.31E–05	9.74E–01	1.46E–01
6H-3, 39	52.89	1.12E–04	1.75E–03	1.13E–02	–1.29E–05	9.87E–01	1.55E–01
6H-3, 59	53.09	1.37E–04	2.13E–03	1.25E–02	–1.26E–05	9.84E–01	1.71E–01
6H-3, 79	53.29	2.54E–04	3.14E–03	2.10E–02	–1.18E–05	9.89E–01	1.50E–01
6H-3, 99	53.49	7.10E–05	1.50E–03	9.40E–03	–1.31E–05	9.96E–01	1.60E–01
6H-3, 119	53.69	1.01E–03	2.69E–03	1.95E–02	–1.16E–05	9.85E–01	1.38E–01
6H-3, 140	53.90	6.46E–05	1.40E–03	8.51E–03	–1.28E–05	9.88E–01	1.64E–01
6H-4, 19	54.19	7.94E–05	1.28E–03	7.49E–03	–1.31E–05	9.84E–01	1.71E–01
6H-4, 39	54.39	9.48E–05	2.21E–03	1.43E–02	–1.26E–05	9.92E–01	1.54E–01
6H-4, 59	54.59	1.14E–04	2.11E–03	1.30E–02	–1.25E–05	9.83E–01	1.62E–01
6H-4, 79	54.79	9.76E–05	2.86E–03	1.99E–02	–1.13E–05	9.89E–01	1.44E–01
6H-4, 99	54.99	1.63E–04	2.44E–03	1.61E–02	–1.26E–05	9.84E–01	1.52E–01
6H-4, 119	55.19	1.94E–04	3.04E–03	1.93E–02	–1.18E–05	9.87E–01	1.57E–01
6H-4, 140	55.40	1.02E–04	2.10E–03	1.40E–02	–1.22E–05	9.87E–01	1.50E–01
6H-5, 19	55.69	1.78E–04	2.37E–03	1.57E–02	–1.19E–05	9.96E–01	1.51E–01
6H-5, 39	55.89	4.35E–05	1.91E–03	1.30E–02	–1.20E–05	9.95E–01	1.47E–01
6H-5, 59	56.09	1.08E–04	2.68E–03	1.65E–02	–1.14E–05	9.86E–01	1.63E–01
6H-5, 79	56.29	5.99E–04	2.70E–03	1.77E–02	–1.18E–05	9.86E–01	1.52E–01
6H-5, 89	56.39	1.52E–04	1.99E–03	1.21E–02	–1.24E–05	9.84E–01	1.64E–01

Note: NRM = natural remanent magnetization, ARM = anhysteretic remanent magnetization, IRM = isothermal remanent magnetization.

continuous record for the late Pleistocene to Holocene. The variability curves of the remanent intensity of ARM and IRM are similar to each other and show cyclic change on 1- to 10-m scales.

Unlithified mudstones to unlithified wackestones lithofacies dominate in the interval above 26.0 mbsf. Several coarse-grained layers such as floatstone-packstone contain abundant *Halimeda* debris, bivalves, gastropods, echinoderms, encrusting red algae, foraminifers, and pteropods intercalated in these sediments. The uppermost packstone layer appears at Sections 166-1003A-2H-4 and 2H-5. High intensities of remanent magnetization occur at the same interval (Fig. 5). The intervals of high intensities of remanent magnetization are observed in Sections 166-1003A-3H-1 and 3H-4 (Fig. 5) and are characterized by coarse-grained floatstone-packstone intervals.

DISCUSSION

Four types of magnetic behavior have been recognized within sediments of the top six cores at Site 1007. They reflect differences in magnetic mineralogy and grain size of magnetic minerals within the sediment. A steep initial increase in the IRM acquisition indicates dominance of low-coercivity magnetic phases like magnetite and maghemite. A gradual rise in IRM acquisition seen in some samples indicates that a high-coercivity phase such as hematite is also present. The lower coercivity of IRM compared to ARM suggests a predominance of finer grained magnetic minerals like single domain or pseudo-single domain (Lowrie and Fuller, 1971; Johnson et al., 1975). The present results indicate that sediment of magnetic Type 2 is dominated by high-coercivity magnetic minerals, whereas those of magnetic Types 1, 3, and 4 are dominated by a low-coercivity phases. The grain size of magnetic minerals varies from one type to another. The dominant magnetic minerals of Type 1 are estimated to be of single- or pseudo-single–domain size. Types 3 and 4 mainly contain multidomain states with slight variations between them.

The interval below 12 mbsf is characterized by meter-scale cyclic changes of light-colored nannofossil ooze to dark-colored unlithified mudstone and wackestone. The top of Site 1006 (0–128 mbsf), ~17 km offshore, consists of a lithology with similar cyclic changes. The

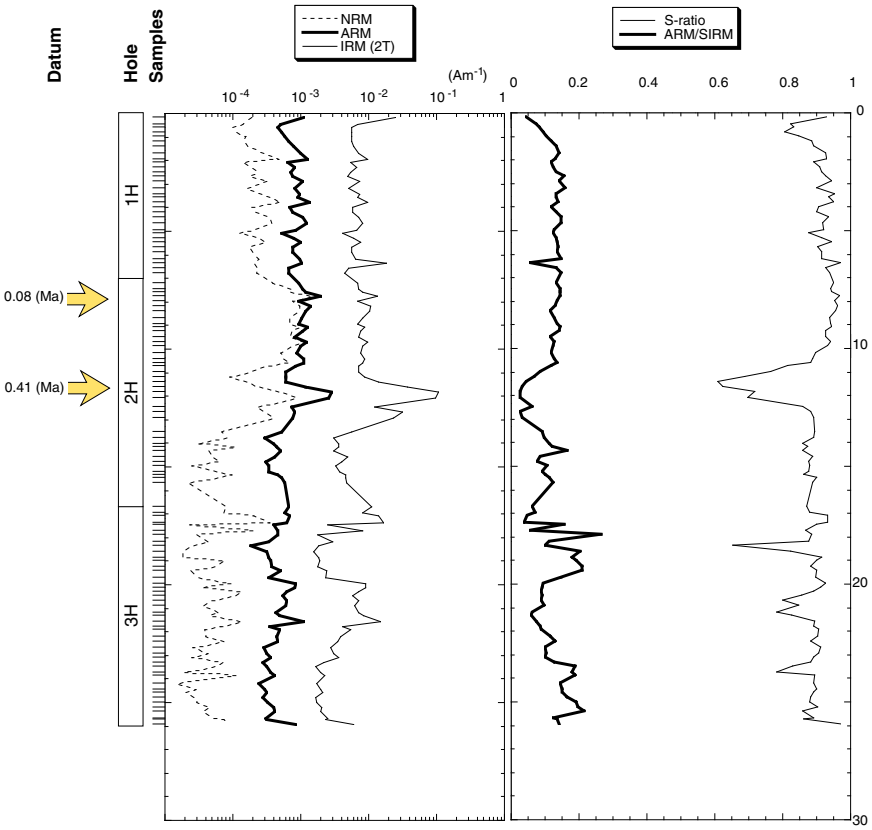

Figure 5. The remanent intensities of NRM, ARM, and IRM (2T) at Site 1003. The right panel shows the S-ratio and ARM/SIRM. ARM = anhysteretic remanent magnetization, IRM = isothermal remanent magnetization, SIRM = saturation isothermal remanent magnetization, NRM = natural remanent magnetization.

clay-rich intervals reflect redeposition of eroded siliciclastics during lowstands of sea level. Light-colored nannofossil ooze lithofacies reflect pelagic sedimentation during highstands of sea level (see Eberli, Swart, Malone, et al., 1997). Relatively high magnetic remanent intensities are observed in this clay-rich interval.

Magnetic mineralogy changes precipitously to a high-coercivity phase (Type 2) with the facies change at 12 mbsf. This conversion in magnetic properties agrees well with the intervals in which sedimentation rate begins to change. We believe that below 12 mbsf, Site 1007 is characterized by pelagic sedimentation, as is the offshore Site 1006 (at present). Progradation of the Bahamas carbonate platform had not developed to the sampling site since this interval (~1.2 Ma). The sedimentation rate of this interval is relatively constant before ~1.2 Ma (Fig. 2). After progradation developed at Site 1007, the current of the Straits of Florida (Santaren Channel) washed out the drift sediment, including the low-coercivity magnetic minerals. An accumulation of mass-gravity flow from the bank is seen within sediments between 2 and 12 mbsf.

An abrupt change from magnetic Types 1 and 2 occurs between Samples 166-1007B-1H-2, 39 cm, and 1H-2, 59 cm (~2 mbsf), comparable to the same intervals of a hiatus between 0.08 and 0.41 Ma. Magnetic minerals above 2 mbsf change completely to a low-coercivity phase with remanent intensity differing by an order of 10^2–10^3. White to light gray nannofossil ooze facies gradually change downhole into a white to pale yellow unlithified foraminifer wackestone to packstone lithofacies in Section 166-1007B-1H-1 (top of core) through Sample 166-1007B-1H-2, 40 cm. The first recorded turbidite occurs at the base of this interval. This turbidite is marked by a sharp erosional basal contact that is overlain by graded unlithified bioclastic grainstone. The basal unlithified grainstone contains fine to medium sand-sized neritic carbonate grains. The average sedimentation rate in this interval is estimated to be >2.5 cm/k.y.

McNeill et al. (1993) relates a decrease in magnetic intensity with depth in the carbonate sediment at the core top to the oxidation of magnetite to maghemite. More detailed study is necessary in order to trace the origin of the magnetic mineral after 0.08 Ma. Many means to obtain magnetic minerals from sediments ranging from siliciclastic, authigenic, diagenetic, and biogenic can be considered. The presence of a hiatus in the same interval reflects different processes of accumulation below and above 2 mbsf.

Remanent intensities of ARM and IRM (applied field = 2 T) plotted against the age of sediments based on the calcareous nannofossil biostratigraphy are shown in Figure 6. High intensities appear above the hiatus. Relatively low intensities of remanent magnetization characterize sediments accumulated from before 1.2 Ma to the hiatus. The variability curve of the magnetic remanent intensities shows cyclic changes, especially after 1.2 Ma, within an interval of relatively constant sedimentation rate (Fig. 6). A high-amplitude variability curve is observed between 1.2 and 1.5 Ma, with a tendency to decrease downward in the core. Some studies of magnetic remanent intensities suggest that high concentrations of magnetic minerals are found during glacial periods, and their record is controlled by glacial–interglacial cycles (e.g., Robinson, 1986; Thouveny et al., 1994; Arai et al, 1997). We compared our variability curve with the oxygen isotope curve of Wei (1993). The amplitude of the variability curve is similar to the oxygen isotope curve (Fig. 6). We need more substantiation and a comparison with the oxygen isotope curve from the present site, however.

In the cores at Site 1003, relatively high intensities of remanent magnetization appear within coarse-grained floatstone-packstone layers. The magnetic signals also show the decrease of finer grained magnetic minerals in the coarse-grained layers, based on the ratio of ARM to SIRM (see Fig. 5, right panel). The sediments of coarse-grained layers are characterized by high amounts of neritic grain (e.g., *Halimeda* debris) export from the platform and are distinguished by a high concentration of relatively coarse-grained magnetic minerals. The fact that variations of magnetic remanent intensity are well correlated with sedimentary lithofacies suggests that the cy-

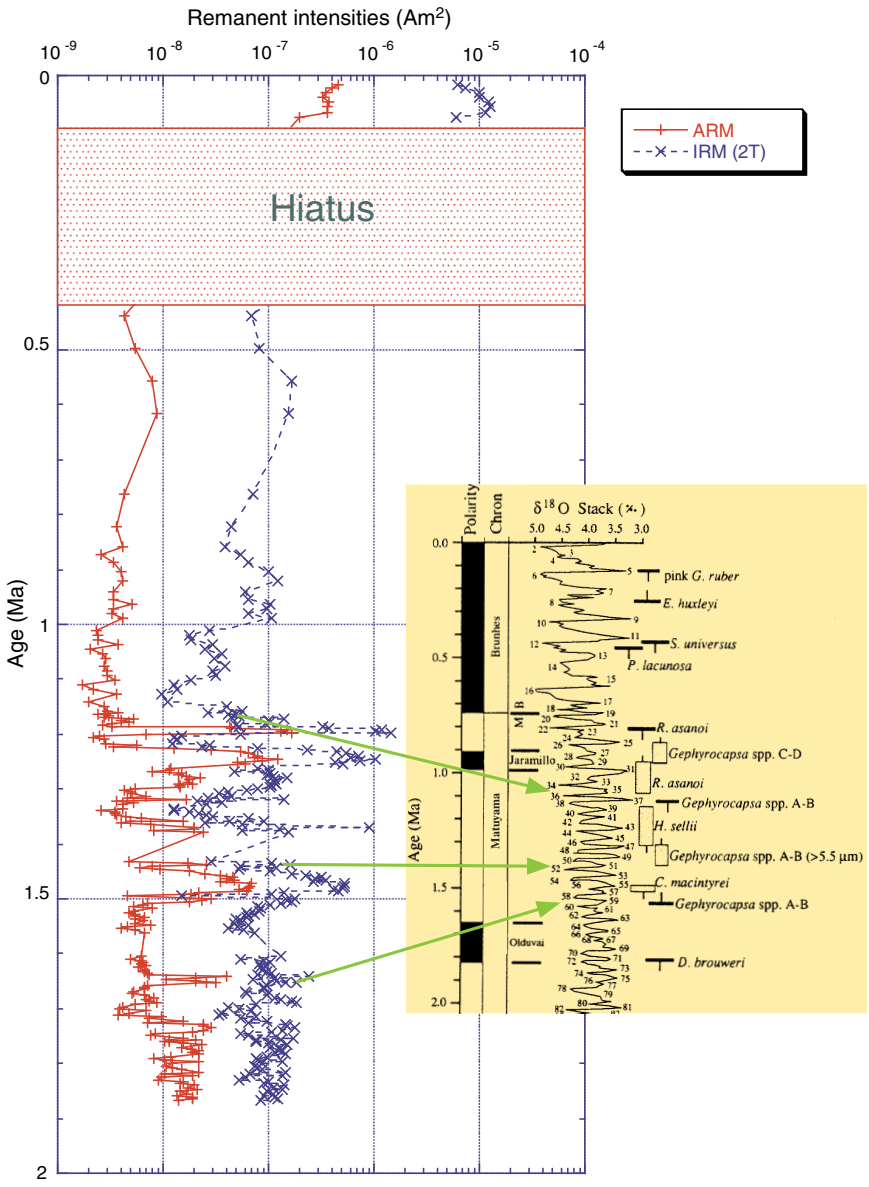

Figure 6. Remanent intensities of ARM and IRM plotted against age of core from Site 1007 based on the calcareous nannofossil biostratigraphy. The curve is compared with the oxygen isotope curve after Wei (1993). ARM = anhysteretic remanent magnetization, IRM = isothermal remanent magnetization.

clic variability curve is dependent on the change of sedimentary processes of the margin of the Great Bahama Bank. The present magnetic studies seem to be useful for revealing the enhancement of effects from the platform. The variability curves at both Sites 1003 and 1007 seem to depend on the amounts of the same origin of magnetic minerals within the sediments. More extensive analyses are necessary to substantiate this contention.

CONCLUSIONS

The results of our study are summarized as follows:

1. Nine calcareous nannofossil events defined by Takayama and Sato (1987) were found within sediments of the top six cores at Site 1007. The sedimentation rate dramatically drops at depths above 12 mbsf, and a hiatus characterized by sharp erosional contact exists at 2 mbsf.
2. The sediments of the top six cores at Site 1007 can be divided into four types based on the IRM acquisition and on the AF demagnetization of ARM and IRM. Two significant magnetic conversion points are found at ~2 and ~12 mbsf (during the Pleistocene).
3. These conversion points seem to reflect changes in oceanic conditions of the slope of the Bahama carbonate platform. They are marked by lithofacies and sedimentation rate changes in the same interval.
4. These results confirm that high-resolution analyses of magnetic properties could be used as an effective indicator of paleoceanography.

ACKNOWLEDGMENTS

We thank many of the scientific staff on the *JOIDES Resolution* for their support of this work. In particular, we are pleased to acknowledge the help of Gregor P. Eberli, Peter K. Swart (co-chief scientists), and Mitchell J. Malone (staff scientist). We would also like to thank Donald F. McNeill and Paul Montgomery for their suggestions and help during sampling and Hirokuni Oda and Hideo Sakai

for their helpful suggestions. We thank Abdelaziz L. Abdeldayem for his constructive criticism of the manuscript. We appreciate the reviews, which helped to greatly improve the manuscript.

REFERENCES

Arai, K., Sakai, H., and Konishi, K., 1997. High-resolution rock-magnetic variability in shallow marine sediment: a sensitive paleoclimatic metronome. *Sediment. Geol.,* 110:7–23.

Bloemendal, J., and deMenocal, P., 1989. Evidence for a change in the periodicity of tropical climate cycles at 2.4 Myr from whole-core magnetic susceptibility measurements. *Nature,* 342:897–900.

Bloemendal, J., Lamb, B., and King, J., 1988. Paleoenvironmental implications of rock-magnetic properties of late Quaternary sediment cores from the eastern equatorial Atlantic. *Paleoceanography,* 3:61–87.

Eberli, G.P., and Ginsburg, R.N., 1987. Segmentation and coalescence of Cenozoic carbonate platforms, northwestern Great Bahama Bank. *Geology,* 15:75–79.

Eberli, G.P., Swart, P.K., Malone, M.J., et al., 1997. *Proc. ODP, Init. Repts.,* 166: College Station, TX (Ocean Drilling Program).

Johnson, H.P., Lowrie, W., and Kent, D.V., 1975. Stability of anhysteretic remanent magnetization in fine and coarse magnetite and maghemite particles. *Geophys. J. R. Astron. Soc.,* 41:1–10.

Kent, D.V., 1982. Apparent correlation of paleomagnetic intensity and climatic records in deep-sea sediments. *Nature,* 299:538–539.

King, J.W., Banerjee, S.K., Marvin, J., and Özdemir, Ö., 1982. A comparison of different magnetic methods for determining the relative grain size of magnetite in natural materials: some results from lake sediments. *Earth Planet. Sci. Lett.,* 59:404–419.

Lowrie, W., and Fuller, M., 1971. On the alternating field demagnetization characteristics of multidomain thermoremanent magnetization in magnetite. *J. Geophys. Res.,* 76:6339–6349.

McNeill, D.F., Guyomard, T.S., and Hawthorne, T.B., 1993. Magnetostratigraphy and the nature of magnetic remanence in platform/periplatform carbonates, Queensland Plateau, Australia. *In* McKenzie, J.A., Davies, P.J., Palmer-Julson, A., et al., *Proc. ODP, Sci. Results,* 133: College Station, TX (Ocean Drilling Program), 573–614.

Robinson, S.G., 1986. The late Pleistocene paleoclimatic record of North Atlantic deep-sea sediments revealed by mineral-magnetic measurements. *Phys. Earth Planet. Inter.,* 42:22–47.

Takayama, T., and Sato, T., 1987. Coccolith biostratigraphy of the North Atlantic Ocean, Deep Sea Drilling Project Leg 94. *In* Ruddiman, W.F., Kidd, R.B., Thomas, E., et al., *Init. Repts. DSDP,* 94 (Pt. 2): Washington (U.S. Govt. Printing Office), 651–702.

Thompson, R., and Oldfield, F., 1986. *Environmental Magnetism:* London (Allen and Unwin).

Thouveny, N., de Beaulieu, J.-L., Bonifay, E., Creer, K.M., Guiot, J., Icole, M., Johnsen, S., Jouzel, J., Reille, M., Williams, T., and Williamson, D., 1994. Climate variations in Europe over the past 140 kyr deduced from rock magnetism. *Nature,* 371:503–506.

Wei, W., 1993. Calibration of Upper Pliocene-Lower Pleistocene nannofossil events with oxygen isotope stratigraphy. *Paleoceanography,* 8:85–99.

Date of initial receipt: 13 August 1998
Date of acceptance: 28 August 1999
Ms 166SR-121